Nearside−Farside and Local Angular Momentum Analyses of Time-Independent Scattering Amplitudes for the H + D_2 ($v_i = 0$, $j_i = 0$) → HD ($v_f = 3$, $j_f = 0$) + D Reaction†

P. D. D. Monks,‡ J. N. L. Connor,*,‡ and S. C. Althorpe§

School of Chemistry, The University of Manchester, Manchester M13 9PL, England and Department of Chemistry, University of Cambridge, Lensfield Road, Cambridge CB2 1EW, England

Received: May 1, 2007; In Final Form: June 12, 2007

The scattering dynamics of the state-to-state reaction H + D_2 ($v_i = 0$, $j_i = 0$, $m_i = 0$) → HD ($v_f = 3$, $j_f = 0$, $m_f = 0$) + D is investigated, where v_i, j_i, m_i and v_f, j_f, m_f are initial and final vibrational, rotational, and helicity quantum numbers, respectively. We use accurate quantum scattering matrix elements for total energies in the range 1.52−2.50 eV (calculated stepwise in 0.01 eV increments). The theoretical tools used are a nearside−farside (NF) analysis of the partial wave series (PWS) for the scattering amplitude, together with NF local angular momentum (LAM) theory. We find that the backward scattering, which is the energy-domain analog of the time-direct reaction mechanism, is N dominated, whereas the forward scattering (time-delayed analog) is a result of NF interference between the more slowly varying N and F subamplitudes. The LAM analysis reveals the existence of a "trench−ridge" structure. We also resum the PWS up to three times prior to making the NF decomposition. We show that such resummations usually provide an improved physical interpretation of the NF differential cross sections (DCSs) and NF LAMs. We analyze two resummed scattering amplitudes in more detail, where particular values of the resummation parameters give rise to unexpected unphysical behavior in the N and F DCSs over a small angular range. We analyze the cause of this unphysical behavior and describe viable workarounds to the problem. The energy-domain calculations in this paper complement the time-domain results reported earlier by Monks, P. D. D.; Connor, J. N. L.; Althorpe, S. C. *J. Phys. Chem. A* **2006**, *110,* 741.

1. Introduction

Understanding the dynamics of chemical reactions is a topic of fundamental importance in physical chemistry.[1−6] In a previous paper,[7] we studied the time-dependent dynamics of the H + D_2 reaction, which has the interesting property that two reaction mechanisms are present: one time-direct, the other time-delayed (by about 25 fs). We introduced the novel concepts of a cumulative time-evolving differential cross section (DCS) and a cumulative energy-evolving angular distribution.[7] The theoretical techniques used in ref 7 were a general plane wave packet (PWP) theory of molecular scattering[8−14] (reviewed in refs 15 and 16), together with a nearside−farside (NF) decomposition[17−55] (reviewed in refs 6, 46, and 56) of the time-dependent scattering amplitude. We also used the related NF concept of a local angular momentum (LAM).[7,33,34,36,39−41]

The purpose of this paper is to extend and complement the work of ref 7 by studying the time-independent (energy-domain) scattering of the H + D_2 reaction. In particular, the following topics are reported and discussed: (a) We present time-independent DCSs for the following state-to-state reaction;

$$\mathrm{H} + \mathrm{D}_2(v_i = 0, j_i = 0, m_i = 0) \rightarrow \mathrm{HD}(v_f = 0, j_f = 0, m_f = 0) + \mathrm{D}$$

where v_i, j_i, m_i and v_f, j_f, m_f are vibrational, rotational, and helicity quantum numbers for the initial and final states, respectively. We use accurate quantum scattering matrix elements to calculate the DCSs for total energies in the range, E = 1.52(0.01)2.50 eV (the notation $w = x(y)z$ indicates increment w in steps of y, starting from $w = x$ and finishing at $w = z$). Here, E is measured with respect to the classical minimum of the D_2 potential energy curve for the potential energy surface number 2 of Boothroyd et al.[57] We have chosen this state-to-state reaction because it is a well-studied benchmark system[58,59] that exhibits interesting and distinct reaction mechanisms. We studied it from a time-dependent point of view in ref 7. (b) We examine structure in the DCSs using NF theory[7,17−55] and the technique of LAM analysis.[7,33,34,36,39−41] The NF analysis exactly decomposes the scattering amplitude into two subamplitudes, one N and the other F. We can then identify complicated scattering patterns in the DCS as arising from the N subamplitude, from the F subamplitude, or from interference between the N and the F subamplitudes. In a similar yet complementary way, the LAM analysis identifies the full and N,F local angular momenta (or equivalently local impact parameters) that contribute to the scattering at different angles under semiclassical conditions. (c) We utilize a resummation method[25,26,30,32−34,36,39] that lets us resum the partial wave series (PWS) for the scattering amplitude prior to making the NF decomposition. We show that such a resummation usually provides an improved physical interpretation of the N and F subamplitudes and their resulting DCSs and LAMs. Note that no resummation techniques were used in the time-dependent analyses of ref 7. (d) We analyze two resummed scattering amplitudes in more detail, where particular values of the resummation parameters give rise to unexpected unphysical behavior in the N and F DCSs over a

† Part of the special issue "Robert E. Wyatt Festschrift".

* To whom correspondence should be addressed. E-mail: J.N.L.Connor@manchester.ac.uk.

‡ The University of Manchester.

§ University of Cambridge.

10.1021/jp073334k CCC: $37.00
Published on Web 10/11/2007

small angular range. We analyze the cause of this unphysical behavior and describe viable workarounds to the problem.

Section 2 outlines the theoretical methods used, and our computations are described in section 3. We present our NF DCS and NF LAM results in sections 4 and 5, respectively. Section 6 contains our conclusions.

2. Theoretical Methods

A. Scattering Amplitude and NF Decomposition. We begin with the time-independent form of the PWS for the scattering amplitude ($f(\theta_R, E)$) where θ_R is the reactive scattering angle (i.e., the angle between the outgoing HD molecule and the incoming H atom). The $f(\theta_R, E)$ term can be expanded in a basis set of Legendre polynomials, because the initial and final helicity quantum numbers for the state-to-state reaction are both zero. Note that, for simplicity of notation, the initial- and final-state labels have been omitted in the following. We can write eq 1:

$$f(\theta_R, E) = \frac{1}{2ik(E)} \sum_{J=0}^{\infty} (2J+1)\tilde{S}_J(E)P_J(\cos\theta_R) \quad (1)$$

where $k(E)$ is the initial translational wavenumber, J is the total angular momentum quantum number, $\tilde{S}_J(E)$ is a modified energy-dependent scattering matrix element, and $P_J(\bullet)$ is a Legendre polynomial of degree J. The corresponding DCS is given by eq 2.

$$\sigma(\theta_R, E) = |f(\theta_R, E)|^2 \quad (2)$$

We use the Fuller NF decomposition,[60] which lets us write eq 3;

$$f(\theta_R, E) = f_N(\theta_R, E) + f_F(\theta_R, E) \quad (3)$$

where the N and F subamplitudes are defined as eq 4 ($\theta_R \neq 0, \pi$)

$$f_{N,F}(\theta_R, E) = \frac{1}{2ik(E)} \sum_{J=0}^{\infty} (2J+1)\tilde{S}_J(E)Q_J^{(\mp)}(\cos\theta_R) \quad (4)$$

with the $Q_J^{(\mp)}(\bullet)$ term given by eq 5 ($\theta_R \neq 0, \pi$)

$$Q_J^{(\mp)}(\cos\theta_R) = \frac{1}{2}\left[P_J(\cos\theta_R) \pm \frac{2i}{\pi} Q_J(\cos\theta_R)\right] \quad (5)$$

and $Q_J(\bullet)$ is a Legendre function of the second kind of degree J. The corresponding NF DCSs are defined by eq 6 ($\theta_R \neq 0, \pi$);

$$\sigma_{N,F}(\theta_R, E) = |f_{N,F}(\theta_R, E)|^2 \quad (6)$$

$\sigma(\theta_R, E)$ may display complicated behavior when plotted versus θ_R. In this situation, plotting $\sigma_{N,F}(\theta_R, E)$ may help shed light on the dynamics of a reaction, because graphs of $\sigma_{N,F}(\theta_R, E)$ versus θ_R often display simpler behavior. We can then interpret structure in a plot of $\sigma(\theta_R, E)$ as arising from the N contribution to $f(\theta_R, E)$, from the F contribution, or from interference between the N and F subamplitudes.

We define the LAM as eq 7;[33,34,36]

$$\mathrm{LAM}(\theta_R, E) = \frac{\mathrm{d}\arg f(\theta_R, E)}{\mathrm{d}\,\theta_R} \quad (7)$$

where the arg is not necessarily the principal value in order that the derivative be well defined. The corresponding NF LAMs are defined by eq 8:[33,34,36]

$$\mathrm{LAM}_{N,F}(\theta_R, E) = \frac{\mathrm{d}\arg f_{N,F}(\theta_R, E)}{\mathrm{d}\,\theta_R} \quad (8)$$

LAM is measured in units of $\hbar$ and contains information on the total angular momenta that contribute to the scattering at the angle θ_R in the semiclassical limit. LAM is a real (positive or negative) number and is not confined to integer values. Positive values of $\mathrm{LAM}(\theta_R, E)$ result from the anticlockwise motion of arg $f(\theta_R, E)$ as θ_R increases and usually correspond to attractive forces. Similarly, negative values result from the clockwise motion of arg $f(\theta_R, E)$ as θ_R increases, which usually correspond to repulsive forces. These two types of behavior are usually attributable to F and N contributions, respectively.

B. Resummation Theory. Extensive experience has demonstrated[6,7,17−56] that NF analysis is a powerful tool for understanding structure in $\sigma(\theta_R, E)$, because the N and F subamplitudes usually have simpler properties compared to $f(\theta_R, E)$. However, sometimes a NF decomposition can produce oscillatory and rapidly varying N,F DCSs, even though $\sigma(\theta_R, E)$ itself is monotonic and slowly varying with θ_R. In this case, the NF decomposition is not physically meaningful, even though by construction it is mathematically exact.

Now the physical meaning of the $f_{N,F}(\theta_R, E)$ is based on the hypothesis that the PWS, written in terms of $Q_J^{(\mp)}(\cos\theta_R)$, can undergo the same manipulations that are used to derive the semiclassical limit of the full $f(\theta_R, E)$, written in terms of $P_J(\cos\theta_R)$. These manipulations are path deformations in $J + 1/2$ of the integrals into which the PWS can be deformed using the Poisson sum formula or the Watson transformation; they depend on the properties of the individual PWS terms when continued from physical half-integer to real or complex values of $J + 1/2$. Decomposing $P_J(\cos\theta_R)$ into $Q_J^{(\mp)}(\cos\theta_R)$ modifies these properties, possibly leading to unphysical contributions in the $f_{N,F}(\theta_R, E)$, which cancel out in $f(\theta_R, E)$. These contributions often manifest themselves as irregular behavior in plots of $\sigma_{N,F}(\theta_R, E)$ and $\mathrm{LAM}_{N,F}(\theta_R, E)$, or we may obtain values of $\sigma_{N,F}(\theta_R, E)$ that are much larger than $\sigma(\theta_R, E)$.[25,26,32−34]

One solution to the problem of unphysical contributions is to work with a resummed form of the PWS.[25,26,32−34] If we write eq 1 in the more compact form shown in eq 9,

$$f(\theta_R, E) = \frac{1}{2ik(E)} \sum_{J=0}^{\infty} a_J(E)P_J(\cos\theta_R) \quad (9)$$

where $a_J(E)$ is given by $a_J(E) = (2J+1)\tilde{S}_J(E)$, then we can apply the following identity[33,34] (eq 10) [where $a_J^{(0)}(E) \equiv a_J(E)$]

$$\sum_{J=0}^{\infty} a_J^{(i-1)}(E)P_J(\cos\theta_R) = \frac{1}{\alpha_i + \beta_i\cos\theta_R} \sum_{J=0}^{\infty} a_J^{(i)}P_J(\cos\theta_R) \qquad i = 1, 2, 3, \ldots \quad (10)$$

with $\alpha_i + \beta_i \cos\theta_R \neq 0$ and eq 11

$$a_J^{(i)}(E) = \beta_i \frac{J}{2J-1} a_{J-1}^{(i-1)}(E) + \alpha_i a_J^{(i-1)}(E) + \beta_i \frac{J+1}{2J+3} a_{J+1}^{(i-1)}(E) \quad (11)$$

with $a_{-1}^{(i-1)}(E) = 0$. The α_i and β_i are complex-valued resummation parameters independent of J but are dependent

on E. We next observe that if α_i, $\beta_i \neq 0$, then the rhs of eq 10 depends only on the ratio β_i/α_i, and without loss of generality we can assume[33,34] $\alpha_i = 1$ for all i and all E.

Iteration of eq 10 r times lets us write $f(\theta_R, E)$ in the resummed form:

$$f(\theta_R, E) = \frac{1}{2ik(E)}\left(\prod_{i=1}^{r}\frac{1}{1+\beta_i \cos\theta_R}\right)\sum_{J=0}^{\infty} a_J^{(r)}(E)P_J(\cos\theta_R) \tag{12}$$

where r is the order of resummation and $r = 1, 2, 3, ...$ The corresponding NF decomposition is then given by eq 13;

$$f(\theta_R, E) = f_N(\beta_1, \beta_2, ..., \beta_r; \theta_R, E) + f_F(\beta_1, \beta_2, ..., \beta_r; \theta_R, E) \qquad r = 1, 2, 3, ... \tag{13}$$

where the N,F resummed subamplitudes are given by eq 14.

$$f_{N,F}(\beta_1, \beta_2, ..., \beta_r; \theta_R, E) = \frac{1}{2ik(E)}\left(\prod_{i=1}^{r}\frac{1}{1+\beta_i \cos\theta_R}\right)\sum_{J=0}^{\infty} a_J^{(r)}(E)Q_J^{(\mp)}(\cos\theta_R) \tag{14}$$

Note that eqs 10, 12, and 14 use an abbreviated notation in which $a_J^{(r)}(E) \equiv a_J^{(r)}(\beta_1, \beta_2, ..., \beta_r; E)$ and $a_J^{(r-1)}(E) \equiv a_J^{(r-1)}(\beta_1, \beta_2, ..., \beta_{r-1}; E)$. The N,F resummed DCSs and LAMs are then defined by eqs 15 and 16.

$$\sigma_{N,F}(\beta_1, \beta_2, ..., \beta_r; \theta_R, E) = |f_{N,F}(\beta_1, \beta_2, ..., \beta_r; \theta_R, E)|^2 \tag{15}$$

$$LAM_{N,F}(\beta_1, \beta_2, ..., \beta_r; \theta_R, E) = \frac{d \arg f_{N,F}(\beta_1, \beta_2, ..., \beta_r; \theta_R, E)}{d\,\theta_R} \tag{16}$$

In the following, we will sometimes use the notation $\boldsymbol{\beta} \equiv (\beta_1, \beta_2, ..., \beta_r)$, as well as the convention that $r = 0$ means the unresummed form of eq 9 is regained.

To determine the β_i, we follow the prescription in ref 33 and equate to zero the first r coefficients, $a_J^{(r)}(E)$ (with $J = 0, 1, 2, ..., r - 1$), and then solve r simultaneous equations of degree r in the $\beta_1, \beta_2, ..., \beta_r$. It is found[33] that for $r = 1$,

$$\beta_1 = -3a_0/a_1 \tag{17}$$

where the argument E has been omitted from the $\beta_1(E)$ and $a_J(E)$, as well as the following equations for simplicity of notation. For $r = 2$, we have eq 18;[33]

$$\beta_{1,2} = (B \pm \sqrt{B^2 - 4A})/2 \tag{18}$$

where A and B are solutions of the linear equations given by eq 19;

$$\begin{cases}\left(\frac{1}{3}a_0 + \frac{2}{15}a_2\right)A + \frac{1}{3}a_1 B = -a_0 \\ \left(\frac{3}{5}a_1 + \frac{6}{35}a_3\right)A + \left(a_0 + \frac{2}{15}a_2\right)B = -a_1\end{cases} \tag{19}$$

and for $r = 3$, the simultaneous linear equations are given by eq 20;

$$\begin{cases}\left(\frac{1}{3}a_1\right)A + \left(\frac{1}{3}a_0 + \frac{2}{15}a_2\right)B + \left(\frac{1}{5}a_1 + \frac{2}{35}a_3\right)C = -a_0 \\ \left(a_0 + \frac{2}{5}a_2\right)A + \left(\frac{3}{5}a_1 + \frac{6}{35}a_3\right)B + \left(\frac{3}{5}a_0 + \frac{12}{35}a_2 + \frac{8}{105}a_4\right)C = -a_1 \\ \left(\frac{2}{3}a_1 + \frac{3}{7}a_3\right)A + \left(\frac{2}{3}a_0 + \frac{11}{21}a_2 + \frac{4}{21}a_4\right)B + \left(\frac{4}{7}a_1 + \frac{1}{3}a_3 + \frac{20}{231}a_5\right)C = -a_2\end{cases} \tag{20}$$

where

$$A = \beta_1 + \beta_2 + \beta_3$$
$$B = \beta_1\beta_2 + \beta_2\beta_3 + \beta_1\beta_3$$
$$C = \beta_1\beta_2\beta_3 \tag{21}$$

The simultaneous eqs 20 and 21 for $r = 3$ are implied in refs 33 and 34, but this is their first explicit statement. A, B, and C will be recognized as the elementary symmetric polynomials in three variables. The analytic solutions of eqs 20 and 21 are not simple, so in practice we solve eqs 20 and 21 numerically for $\beta_1, \beta_2, \beta_3$.

For the above choice of the parameters β_i, $i = 1, 2, 3 ...$, increasing the value of r has the effect of moving numerically significant terms[32−34,36,39] from low values of J to larger values of J. This concentrating effect, which emphasizes partial waves with $J \gg 1$, favors a physically meaningful NF analysis, because the $Q_J^{(\pm)}(\cos\theta_R)$ become traveling angular waves in this limit,[7,20] namely, eq 22.

$$Q_J^{(\pm)}(\cos\theta_R) \sim \left[2\pi\left(J+\frac{1}{2}\right)\sin\theta_R\right]^{-1/2} \exp\left\{\pm i\left[\left(J+\frac{1}{2}\right)\theta_R - \frac{1}{4}\pi\right]\right\} \tag{22}$$

In practice, the N,F DCSs and N,F LAMs are calculated for $r = 0$, 1, 2, and 3. Then one typically sees convergent behavior of the N,F curves over larger and larger angular ranges as r increases.[32−34,36,39] Sometimes it is found that the $r = 0$ and $r = 1$ curves agree, and it is then not necessary to go to the $r = 2$ and $r = 3$ cases (although these will provide additional checks). The r-increasing algorithm just described has also been compared with semiclassical results for the N,F DCSs and N,F LAMs, and close agreement has been found.[32−34,36,39]

In a few examples, which are discussed in Section 4D, we find unphysical behavior in the N and F DCSs over a small angular range. Section 4E provides a workaround to this problem. It should also be noted that the resummed $f(\theta_R, E)$ (eq 12) is independent of the β_i and remains unchanged with increasing r, because any unphysical contributions to the $f_{N,F}(\boldsymbol{\beta}; \theta_R, E)$ cancel out. Also, the resummation theory described above applies equally to the time-dependent PWS for the scattering amplitude ($f(\theta_R, t)$) used in ref 7.

3. Calculations

Our input is the same as in ref 7, namely, accurate quantum scattering matrix elements, $\tilde{S}_J(E)$, for $J = 0(1)30$ on the energy grid, $E = 1.52(0.01)2.50$ eV. The total energy E is measured with respect to the classical minimum of the D_2 potential energy curve. These matrix elements are the results of scattering calculations performed for the indistinguishable state-to-state reaction, $H + D_2$ ($v_i = 0$, $j_i = 0$, $m_i = 0$) → HD ($v_f = 3$, $j_f = 0$, $m_f = 0$) + D, using the potential energy surface number 2 of Boothroyd et al.[57] with masses of $m_H = 1.008$ u and $m_D = 2.014$ u. Our computations used a state-to-state wave packet method,[61] which has previously been applied to several other reactions.[8−12,15,16,50−53,61−66]

Because the rovibrational energy, $E(v_i, j_i)$, of D_2 ($v_i = 0$, $j_i = 0$) is 0.192 eV and the rovibrational energy, $E(v_f, j_f)$, of HD ($v_f = 3$, $j_f = 0$) is 1.520 eV, the reaction is closed for $E < 1.520$ eV. The scattering amplitude was resummed using values of r up to $r = 3$. We specify the value of r in all cases where a resummation has been carried out.

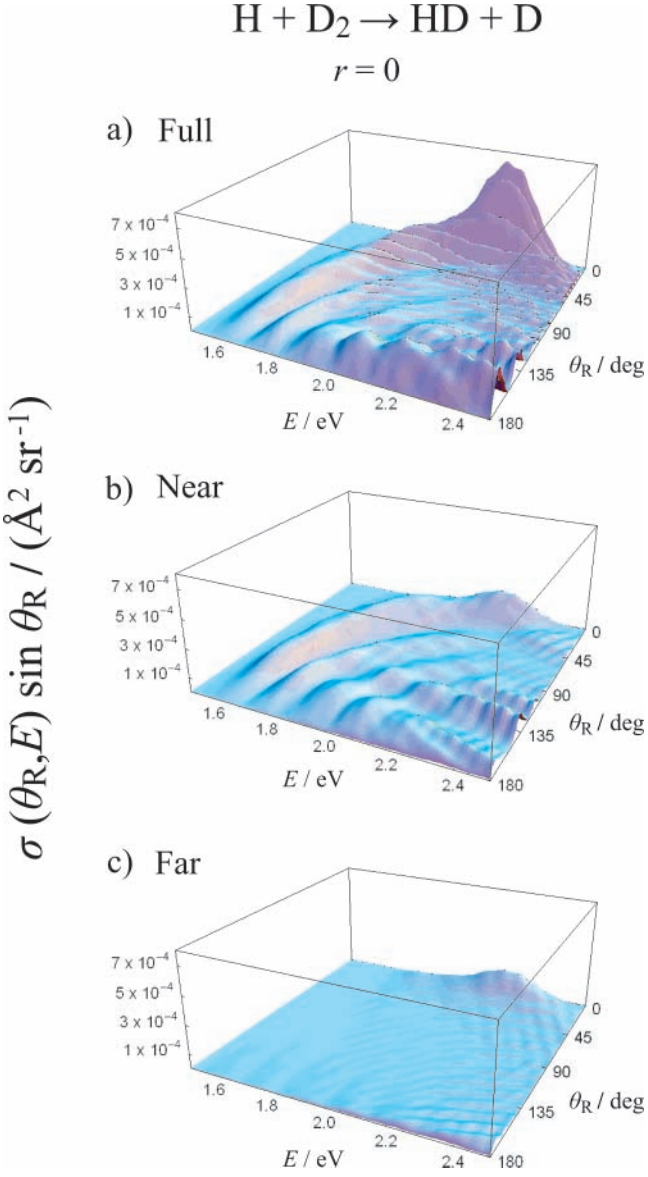

Figure 1. Perspective plots of (a) $\sigma(\theta_R,E)$ sin θ_R, (b) $\sigma_N(\theta_R,E)$ sin θ_R, and (c) $\sigma_F(\theta_R,E)$ sin θ_R vs θ_R and E, all for resummation order, $r = 0$.

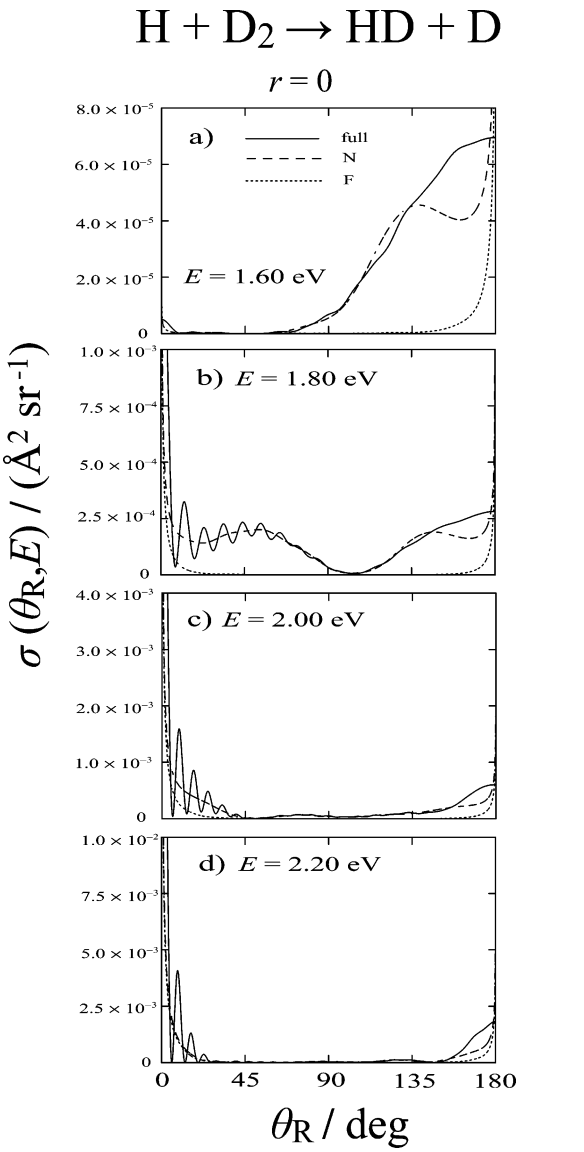

Figure 2. Linear plots of $\sigma(\theta_R, E)$ (solid curve), $\sigma_N(\theta_R, E)$ (dashed curve), and $\sigma_F(\theta_R, E)$ (dotted curve) vs θ_R, all for resummation order, $r = 0$. (a) $E = 1.60$ eV, (b) $E = 1.80$ eV, (c) $E = 2.00$ eV, and (d) $E = 2.20$ eV.

4. Results for NF DCSs

This section presents our results for the resummed N and F DCSs. It is important to note that our discussion of the r dependent N,F DCSs in this section, as well as the r dependent N,F LAMs in Section 5, are supported by the semiclassical N,F analyses in ref 39, which used a J-shifted Eckart parametrization for the scattering matrix element to study the dynamics of the H + D_2 ($v_i = 0$, $j_i = 0$, $m_i = 0$) → HD ($v_f = 3$, $j_f = 0$, $m_f = 0$) + D reaction.

A. NF DCSs for $r = 0$. Perspective plots of $\sigma(\theta_R, E)$, $\sigma_N(\theta_R, E)$, and $\sigma_F(\theta_R, E)$ are presented in Figure 1 for $r = 0$. The DCSs have been multiplied by sin θ_R to contain large features in the scattering close to $\theta_R = 0°$ and 180°. Figure 2 is a more detailed display of some of the results in Figure 1; it shows linear plots of the DCSs at four individual energies, $E = 1.60$, 1.80, 2.00, and 2.20 eV. When $\sigma(\theta_R, E)$, $\sigma_N(\theta_R, E)$, and $\sigma_F(\theta_R, E)$ are small, Figure 2 has the disadvantage that important properties of the DCSs are not visible. Figure 3 displays logarithmic plots at the same four energies to more clearly highlight features of the small DCSs (n.b. no sin θ_R factor is included in Figures 2 and 3). The relation between $\sigma_N(\theta_R, E)$, $\sigma_F(\theta_R, E)$, and $\sigma(\theta_R, E)$ is given by the fundamental NF identity for cross sections, namely, eq 23;[40,60]

$$\sigma(\theta_R, E) = \sigma_N(\theta_R, E) + \sigma_F(\theta_R, E) + 2[\sigma_N(\theta_R, E)\sigma_F(\theta_R, E)]^{1/2} \cos[\arg f_N(\theta_R, E) - \arg f_F(\theta_R, E)] \quad (23)$$

which is also true for the resummed N and F DCSs.

It is evident from Figures 1−3 that the backward (direct) scattering is N dominated, whereas the pronounced forward (delayed) scattering, seen clearly for cases where $E \geq 1.80$ eV in Figures 1−3, displays rapid oscillations as a function of θ_R caused by interference between the more slowly varying N and F subamplitudes. Note that the result for $E = 2.00$ eV has been known for some time; in particular, the semiclassical analyses of refs 35−39 and 47 show that these rapid oscillations are part of a forward glory. There is some F character in the scattering at backward angles (see Figure 2); however, this is likely to be a (well understood) example of the NF decomposition overestimating the F contribution in the backward direction, as previously discussed in ref 23.

The slow undulations observed as a function of E at large angles in the $\sigma(\theta_R, E)$ plots are present in the $\sigma_N(\theta_R, E)$ and so

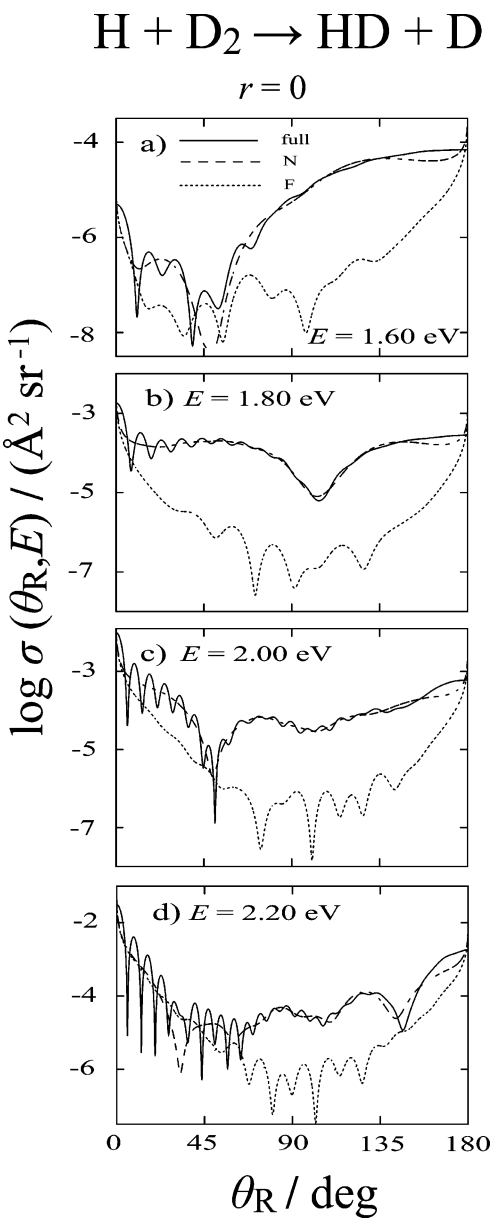

Figure 3. Logarithmic plots of $\sigma(\theta_R, E)$ (solid curve), $\sigma_N(\theta_R, E)$ (dashed curve), and $\sigma_F(\theta_R, E)$ (dotted curve) vs θ_R, all for resummation order, $r = 0$. (a) $E = 1.60$ eV, (b) $E = 1.80$ eV, (c) $E = 2.00$ eV, and (d) $E = 2.20$ eV.

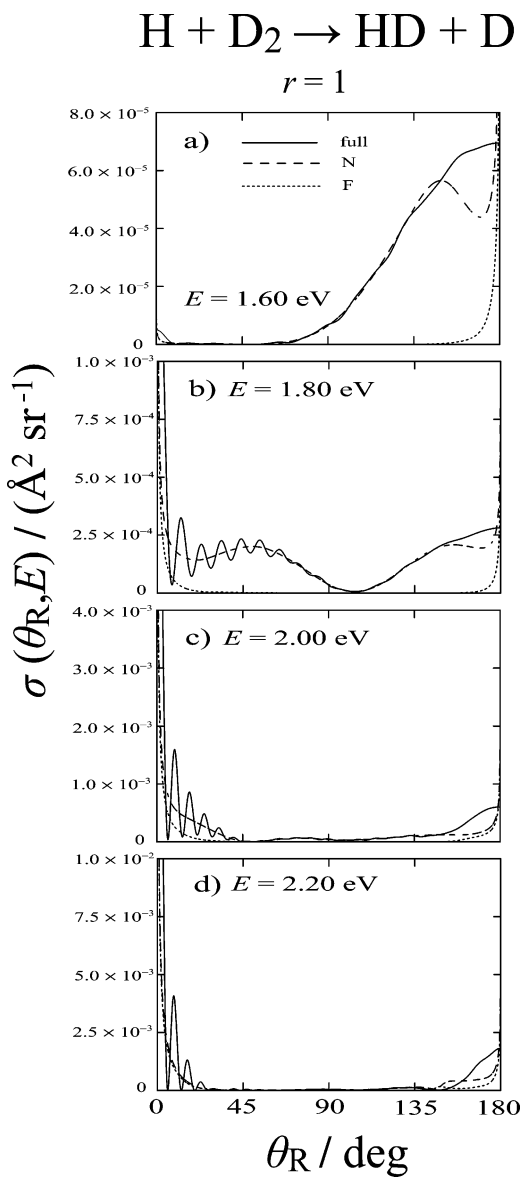

Figure 4. Linear plots of $\sigma(\theta_R, E)$ (solid curve), $\sigma_N(\theta_R, E)$ (dashed curve), and $\sigma_F(\theta_R, E)$ (dotted curve) vs θ_R, all for resummation order, $r = 1$. (a) $E = 1.60$ eV, (b) $E = 1.80$ eV, (c) $E = 2.00$ eV, and (d) $E = 2.20$ eV.

are not a result of NF interference. These oscillations have been attributed[67] to interference between contributions to the overall reaction pathway from the presence of quantized transition states (sometimes called quantum bottleneck states). The slow oscillations observed as a function of θ_R at nearly all energies in the $\sigma(\theta_R, E)$ plots are likewise only present in the $\sigma_N(\theta_R, E)$ and so are also not a NF interference effect.

The results in Figures 1−3 complement the time-dependent findings of ref 7.

B. NF DCSs for $r = 1$. Figures 4 and 5 illustrate the effect on the N,F DCSs of resumming ($r = 1$) the PWS for the scattering amplitude, at the same four energies as in Section 4A for linear and logarithmic plots, respectively. On comparing Figures 2 and 4, we do not see any meaningful differences in the N,F curves for $r = 0$ and $r = 1$, respectively. This illustrates, for these (relatively) large N,F DCSs, the convergence that was described in Section 2B as r increases. Next, we compare Figure 3 for $r = 0$ with Figure 5 for $r = 1$ to see whether resumming the scattering amplitude ($r = 1$) has the effect of "cleaning" the (relatively) small $r = 0$ $\sigma_F(\theta_R, E)$ curve (i.e., unphysical features are removed or are less apparent, resulting in smoother, more regular N,F curves when $r = 1$). Also, complicated structure is often shifted to larger values of θ_R as r changes from $r = 0$ to $r = 1$, which is an indication that resummation has improved the physical usefulness of the NF decomposition.[32−34,36,39] We do see a cleaning effect, although only a small one (apart from $\theta_R \approx 150°$ at $E = 2.20$ eV), which demonstrates that the N,F $r = 0$ curves are almost converged.

On the other hand, if spurious features are introduced into the resummed $\sigma_N(\boldsymbol{\beta}; \theta_R, E)$ and $\boldsymbol{\sigma}_F(\boldsymbol{\beta}; \theta_R, E)$, then it is a sign that resummation has not contributed any valuable physical insights into understanding structure in $\sigma(\theta_R, E)$ at that specific angle. An example occurs in Figure 5d for $\theta_R \approx 150°$ where the F DCS becomes larger than the N DCS over a small angular range. This is a (mild) example of the unphysical behavior that is analyzed later in section 4D. By following the remedy described in section 4E, Figure 5d can be cleaned; the result for $\theta_R \approx 150°$ (not shown) then looks similar to the $r = 0$ N,F curves in Figure 3d. Note that in both the resummed and the

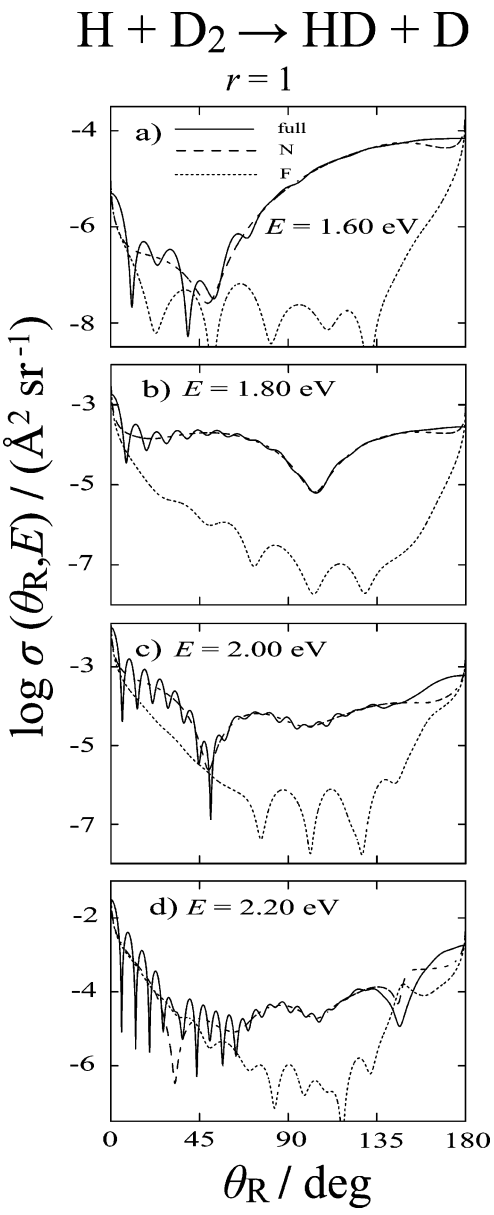

Figure 5. Logarithmic plots of $\sigma(\theta_R, E)$ (solid curve), $\sigma_N(\theta_R, E)$ (dashed curve), and $\sigma_F(\theta_R, E)$ (dotted curve) vs θ_R, all for resummation order, $r = 1$. (a) $E = 1.60$ eV, (b) $E = 1.80$ eV, (c) $E = 2.00$ eV, and (d) $E = 2.20$ eV.

unresummed cases the NF decomposition is, by construction, mathematically exact.

C. NF DCSs for $r = 2$ and $r = 3$. The effects of increasing the resummation order from $r = 1$ to $r = 2$ and then to $r = 3$ are presented in Figure 6, panels a and b, respectively, at $E = 2.00$ eV. The logarithmic plots of Figures 5c and 6a clearly show that changing $r = 1$ to $r = 2$ does not necessarily guarantee an improvement in the physical behavior of $\sigma_N(\beta_1, \beta_2; \theta_R, E)$ and $\sigma_F(\beta_1, \beta_2; \theta_R, E)$, because the N,F $r = 2$ DCSs "blow-up" over a small angular range near $\theta_R = 166°$, where they become much larger than $\sigma(\theta_R, E)$. This unexpected feature is unlikely to be physically meaningful, because it disappears in the F DCS and is much reduced in the N DCS when we move to the next order of resummation, $r = 3$, in Figure 6b. The feature is also absent from the $r = 0$ and $r = 1$ plots shown in Figures 2c−5c.

The question naturally arises: what causes the unphysical feature to appear for the $r = 2$ resummation, whereby the N and F DCSs blow-up for $\theta_R \approx 166°$, but not for the $r = 1$ and $r = 3$ resummations? This is analyzed and discussed in the next section.

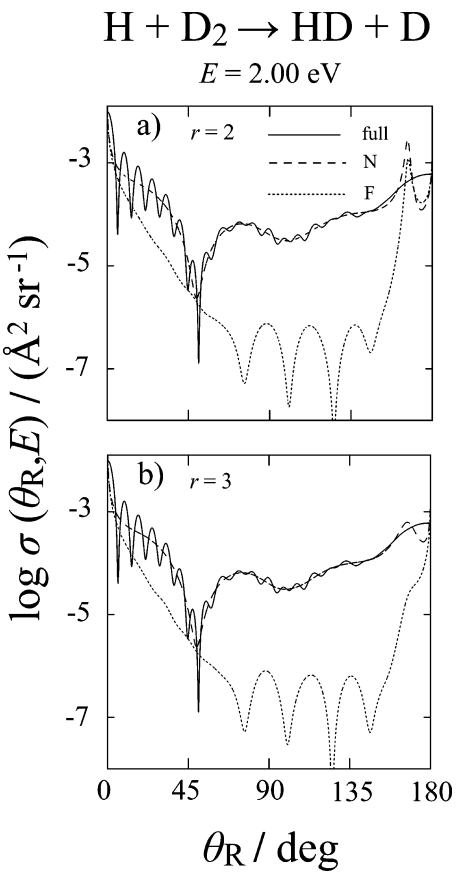

Figure 6. Logarithmic plots of $\sigma(\theta_R, E)$ (solid curve), $\sigma_N(\theta_R, E)$ (dashed curve), and $\sigma_F(\theta_R, E)$ (dotted curve) vs θ_R, for $E = 2.00$ eV and for resummation orders, (a) $r = 2$ and (b) $r = 3$.

TABLE 1: Values of Physical Quantities Entering eqs 10−21[a]

values of resummation parameters and moduli of the presummation factors	
$r = 1$	
β_1	$1.046 - 0.06288i$
$1/\lvert 1 + \beta_1 \cos\theta_R \rvert$	15.89
$r = 2$	
β_1	$1.028 + 0.005613i$
$1/\lvert 1 + \beta_1 \cos\theta_R \rvert$	167.9
β_2	$-1.139 - 0.5392i$
$1/\lvert 1 + \beta_2 \cos\theta_R \rvert$	0.4611
$1/\lvert (1 + \beta_1 \cos\theta_R)(1/\lvert 1 + \beta_2 \cos\theta_R \rvert) \rvert$	77.42
$r = 3$	
β_1	$-1.162 - 0.1179i$
$1/\lvert 1 + \beta_1 \cos\theta_R \rvert$	0.4693
β_2	$1.817 + 1.790i$
$1/\lvert 1 + \beta_2 \cos\theta_R \rvert$	0.5271
β_3	$1.020 + 0.02085i$
$1/\lvert 1 + \beta_3 \cos\theta_R \rvert$	43.70
$1/\lvert (1 + \beta_1 \cos\theta_R)(1 + \beta_2 \cos\theta_R)(1 + \beta_3 \cos\theta_R) \rvert$	10.81

[a] For the H + D_2 reaction at $r = 1$, 2, and 3 for $\theta_R = 166°$ and total energy $E = 2.00$ eV

D. Limitations of the Resummation Method. Table 1 reports, for $r = 1$, 2, and 3, values of the real and imaginary parts of the resummation parameters (β_i) where $i = 1$, 2, or 3 entering eqs 10−21 at $E = 2.00$ eV. Values for the moduli of the presummation factors (e.g., $1/|1 + \beta_1 \cos\theta_R|$) that

contribute to the moduli of the N,F resummed scattering amplitudes (e.g., $|f_{N,F}(\beta_1; \theta_R, E)|$) are also reported for $\theta_R = 166°$.

We see that the moduli of the presummation factors for the $r = 1, 2, 3$ cases are all large, especially for $r = 2$. It is clear that, because the square of these moduli contribute to the final $\sigma_N(\boldsymbol{\beta}; \theta_R, E)$ and $\sigma_F(\boldsymbol{\beta}; \theta_R, E)$, the $r = 2$ case may exhibit significant blow-up behavior around $\theta_R = 166°$, with $r = 1$ and $r = 3$ exhibiting less. It is also apparent from Table 1 that the major contributing term to the large $r = 2$ presummation factor is the $i = 1$ term $(1/|1 + \beta_1 \cos \theta_R)|)$, which is determined by β_1.

Because it is the values of the resummation parameters β_i that probably cause the undesired blow-up behavior, it is necessary to investigate the observation that, although the $r = 3$ case contains three β_i parameters and therefore more potential for unphysical behavior, it is the $r = 2$ case that exhibits the problem. A blow-up to infinity will occur when β_i satisfies eq 24;

$$1 + \beta_i \cos \theta_R = 0 \tag{24}$$

which implies, because θ_R and $\cos \theta_R$ are real, the following: (a) β_i must be real (i.e., Im $\beta_i = 0$) with the value Re $\beta_i = -1/\cos \theta_R$. (b) Because $-1 \le \cos \theta_R \le 1$, it is clear that Re $\beta_i \le -1$ for $0° \le \theta_R < 90°$ and Re $\beta_i \ge +1$ for $90° < \theta_R \le 180°$. At $\theta_R = 90°$, Re β_i jumps from $-\infty$ to $+\infty$.

We see from Table 1 that, for $r = 2$, the value of Im β_1 is very close to zero and Re $\beta_1 > 1$. Equation 24 then predicts (with β_1 replaced by Re β_1) that a blow-up will occur at $\theta_R = 166°$ for $r = 2$ and $E = 2.00$ eV (as is observed). The other values of $|\text{Im } \beta_i|$, for $r = 1$, 2, and 3, are much larger, and so no (or much reduced) blow-up behavior is observed at $E = 2.00$ eV and $\theta_R = 166°$ for $r = 1$ and $r = 3$.

Figure 7 shows, for $r = 1$, plots of Re $\beta_1(E)$ and Im $\beta_1(E)$ versus E for the range 1.52 eV $\le E \le$ 2.50 eV. It can be seen that there are eight energies where Im $\beta_1(E) = 0$. Using these plots, it is possible to predict values of E for which blow-up behavior can occur. For example, Figure 7 shows that Im $\beta_1(E) \approx 0$ and Re $\beta_1(E) > 1$ for $E = 2.18$ eV. Table 2 reports values, for $r = 1$, 2, and 3, of the real and imaginary parts of the resummation parameters $\beta_i(E)$, where $i = 1$, 2, or 3, at $E = 2.18$ eV. Because Re $\beta_1 > 1$ for $r = 1$, it is expected that blow-up behavior will be observed in the DCS at some value of θ_R where $90° < \theta_R < 180°$, which is indeed the case; see Figure 8a. Indeed, eq 24 predicts [with β_1 replaced by Re β_1] that the blow-up will occur near $\theta_R = 153°$, as is observed. It is clear that the values of $\beta_i(E)$ for $r = 2$ and 3, and $i = 1$, 2, and 3 are such that no blow-up behavior is expected at large angles in the graphs of the N,F DCSs when $r = 2$ and 3. Figure 8 shows plots of $\sigma(\theta_R, E)$, $\sigma_N(\boldsymbol{\beta}; \theta_R, E)$ and $\sigma_F(\boldsymbol{\beta}; \theta_R, E)$ for $E = 2.18$ eV and $r = 1$, 2, and 3. We see blow-up behavior at $\theta_R \approx 153°$ for $r = 1$, but none in the $r = 2$ or $r = 3$ graphs, as expected.

To understand the blow-up behavior better, we note that eq 14 can be written with the help of eq 5 in the form given by eq 25;

$$f_{N,F}(\beta_1, \beta_2, ..., \beta_r; \theta_R, E) = \frac{1}{2} f(\theta_R, E) \pm \frac{1}{2ik(E)} \left(\prod_{i=1}^{r} \frac{1}{1 + \beta_i \cos \theta_R} \right) \sum_{J=0}^{\infty} a_J^{(r)}(E) Q_J(\cos \theta_R) \tag{25}$$

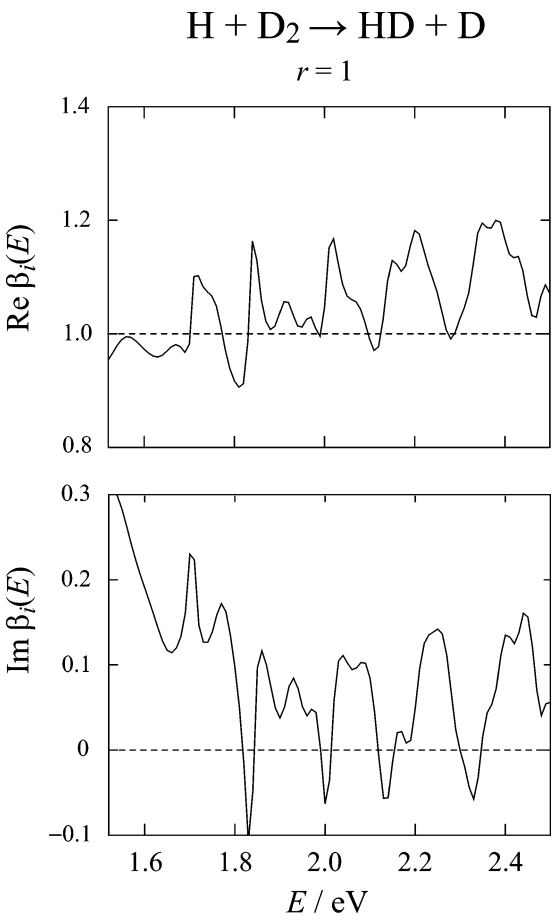

Figure 7. Plots of Re $\beta_i(E)$ and Im $\beta_i(E)$ vs E for resummation order, $r = 1$.

TABLE 2: Values of Resummation Parameters Entering eqs 10−21[a]

	values of resummation parameters
	$r = 1$
β_1	1.120 + 0.008247i
	$r = 2$
β_1	1.085 + 0.04298i
β_2	−0.8995 − 0.1564i
	$r = 3$
β_1	−1.059 + 0.008917i
β_2	1.025 + 0.04377i
β_3	1.095 + 0.2875i

[a] For the H + D_2 reaction for $r = 1$, 2, and 3 at a total energy $E = 2.18$ eV

where the resummed $f(\theta_R, E)$ is given by eq 12. Now, if we compute the resummed $f(\theta_R, E)$ using eq 12, we obtain the same numerical result as the un-resummed PWS (eq 9). This shows that the large values of the presummation factors in the resummed eq 12 do not cause blow-ups in the computation of the (resummed) $f(\theta_R, E)$. Hence, the blow-ups must arise mainly from the second term in eq 25. We have verified that this is indeed the case by plotting the modulus of the second term versus θ_R. The behavior just described can be understood by noting that the $P_J(\cos \theta_R)$ in eq 12 are bounded $(-1 \le P_J(\cos \theta_R) \le +1)$, whereas this is not true for the $Q_J(\cos \theta_R)$ term. Rather, we can have $|Q_J(\cos \theta_R)| > 1$ at small and large angles, as illustrated in Figure 15 of ref 20.

E. A Simple Way to Overcome Limitations of the Resummation Method. In the resummation theory, the values of the resummation parameters $\beta_i(E)$ are arbitrary (provided 1 +

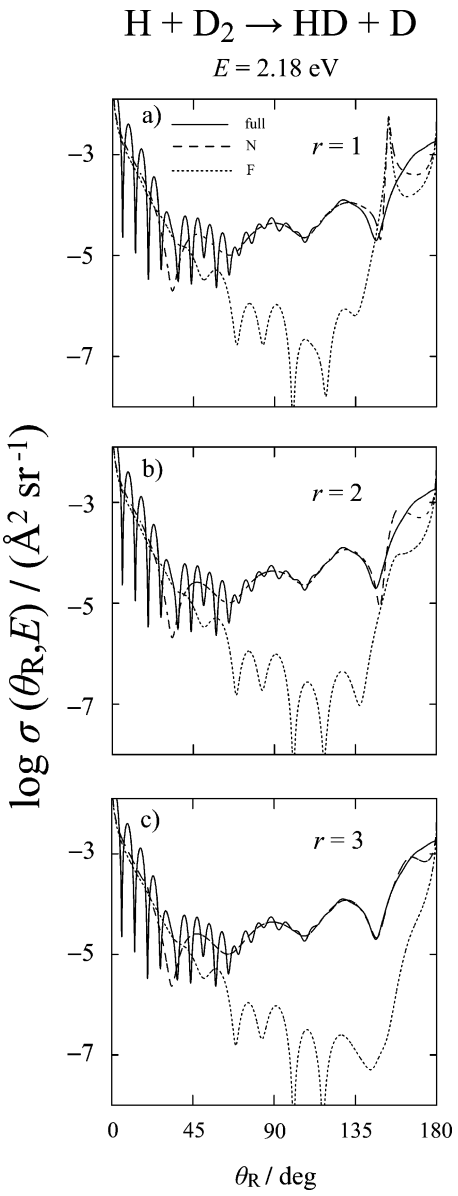

Figure 8. Logarithmic plots of $\sigma(\theta_R, E)$ (solid curve), $\sigma_N(\theta_R, E)$ (dashed curve), and $\sigma_F(\theta_R, E)$ (dotted curve) vs θ_R, for $E = 2.18$ eV and for resummation orders, (a) $r = 1$, (b) $r = 2$, and (c) $r = 3$.

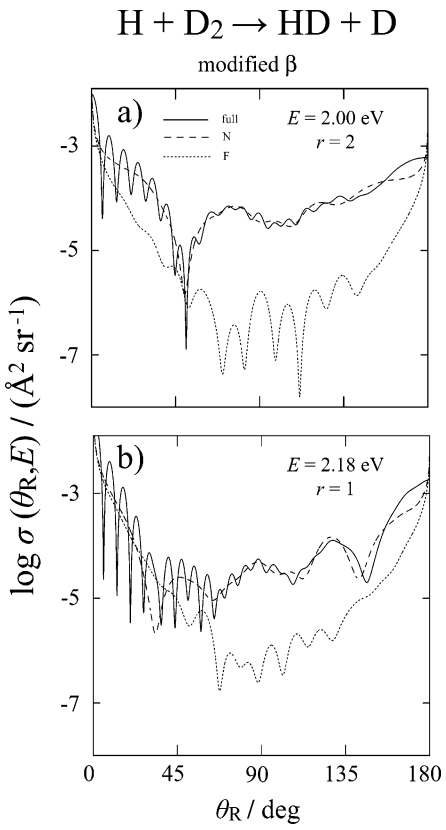

Figure 9. Logarithmic plots of $\sigma(\theta_R, E)$ (solid curve), $\sigma_N(\theta_R, E)$ (dashed curve), and $\sigma_F(\theta_R, E)$ (dotted curve) vs θ_R, for (a) $E = 2.00$ eV and $r = 2$ and (b) $E = 2.18$ eV and $r = 1$. Both use modified values of the resummation parameters $\beta_i(E)$, as described in Section 4E.

$\beta_i(E) \cos \theta_R \neq 0$) and can be changed to reduce the presence of unphysical contributions. For example, the analysis in Section 4D suggests that we should move the imaginary part of $\beta_i(E)$ away from zero for those presummation factors that display blow-up behavior. Figure 9 presents DCSs that result from adding +i to the $\beta_i(E)$ parameters that produce the two blow-up cases in Figures 6a ($E = 2.00$ eV, $r = 2$) and 8a ($E = 2.18$ eV, $r = 1$). The modified values of $\beta_i(E)$ are $\beta_1 = 1.028 + 1.006$i, $\beta_2 = -1.139 - 0.5392$i for $E = 2.00$ eV and $r = 2$, and $\beta_1 = 1.120 + 1.008$i for $E = 2.18$ eV and $r = 1$. It is clear that the undesired behavior of the N and F DCSs has been reduced dramatically for both cases. It would be possible to automate this procedure by adjusting the Im $\beta_i(E)$ when the closeness of the Im $\beta_i(E)$ to zero means there is potential for blow-ups (e.g., when $|\text{Im } \beta_i(E)| \leq 0.01$ for $|\text{Re } \beta_i(E)| > 1$).

5. Results for NF LAMs

Next, we present contour plots of $\text{LAM}(\theta_R, E)$, $\text{LAM}_N(\theta_R, E)$ and $\text{LAM}_F(\theta_R, E)$ (with no resummation) for the ranges $0° < \theta_R < 180°$ and $1.52 \text{ eV} \leq E \leq 2.50$ eV in Figure 10, panels a−c, respectively. Plots of the full and N,F LAMs at the same four values of E used in Section 4, namely, $E = 1.60$, 1.80, 2.00, and 2.20 eV, are shown in Figures 11 and 12 for $r = 0$ and $r = 1$, respectively.

We first consider the general trends in Figure 10. Upon studying the $\text{LAM}_N(\theta_R, E)$ contour plot in Figure 10b, the existence of a distinctive, well-defined feature is immediately apparent. This feature, drawn as a red curve, is a pronounced negative "trench" starting from approximately ($\theta_R = 180°$, $E = 1.70$ eV) and moving through the (θ_R, E) plane to approximately ($\theta_R = 45°$, $E = 2.05$ eV), at which point the trench becomes a pronounced positive "ridge" structure. At about ($\theta_R = 30°$, $E = 2.20$ eV) it becomes negative again, and although less distinct, it appears to continue to ($\theta_R \approx 0°$, $E \approx 2.50$ eV)]. This "trench−ridge" structure is also visible in the contour plot of $\text{LAM}(\theta_R, E)$ in Figure 10a, where it is again drawn as a red curve. It can be no coincidence that this trench−ridge structure follows a path in the (θ_R, E) plane, which is very similar to the "boundary line" in the time-independent DCS that separates the analogs of the time-direct and time-delayed mechanisms (see the lower two plots either in Figure 3 of ref 9 or in Figure 1 of ref 16).

The (predominantly) N trench−ridge feature may be described as an increased N effect when it takes the form of a trench, and a reduced N effect when it takes the form of a ridge. The latter is unusual in applications of LAM theory in that $\text{LAM}_N(\theta_R, E)$ is usually well behaved (i.e., it is usually negative and slowly varying and not oscillating around zero[33,34]). Resumming the scattering amplitude to $r = 1$ does not remove the trench−ridge structure (see Figure 12), and so it is likely to be a genuine physical phenomenon. The cause of these increased/reduced N effects will be discussed in another paper,

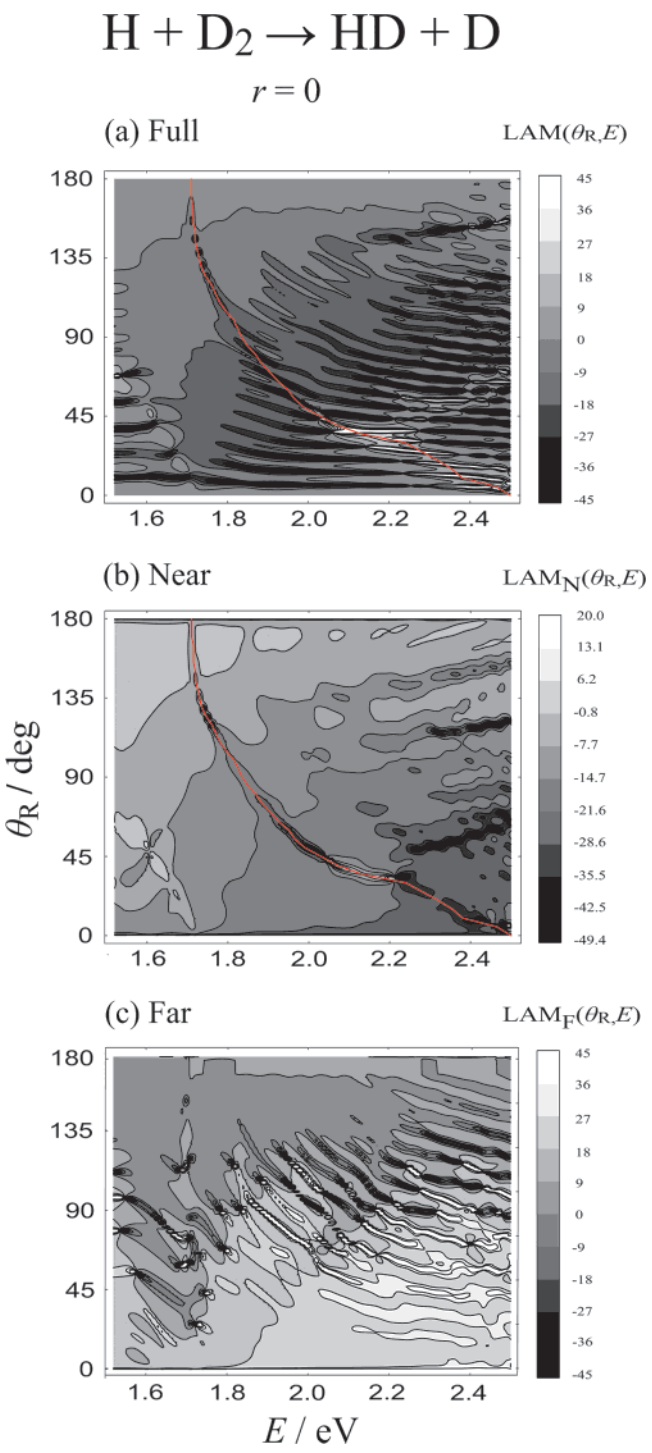

Figure 10. LAM contour plots for resummation order, $r = 0$ of (a) LAM(θ_R, E), where the red curve indicates the trench−ridge structure, (b) LAM$_N$(θ_R, E), where the red curve indicates the trench−ridge structure, (c) LAM$_F$(θ_R, E).

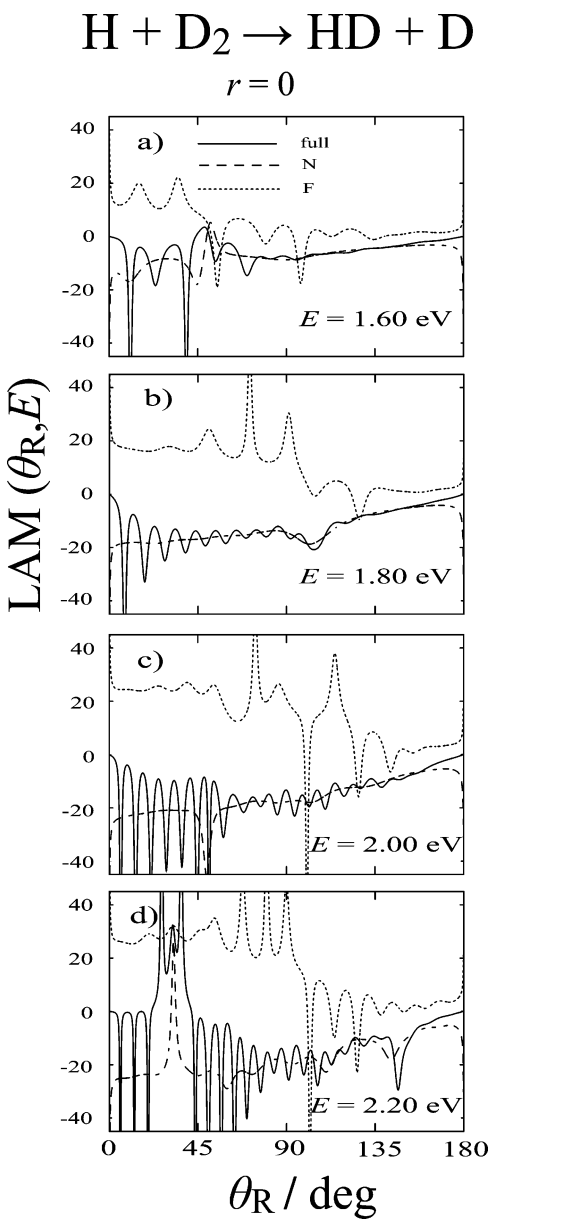

Figure 11. Plots of LAM(θ_R, E) (solid curve), LAM$_N$(θ_R, E) (dashed curve), and LAM$_F$(θ_R, E) (dotted curve) vs θ_R, for resummation order, $r = 0$. (a) $E = 1.60$ eV, (b) $E = 1.80$ eV, (c) $E = 2.00$ eV, and (d) $E = 2.20$ eV. The trench−ridge structure occurs at (b) $\theta_R \approx 104°$ for $E = 1.80$ eV, (c) $\theta_R \approx 50°$ for $E = 2.00$ eV, and (d) $\theta_R \approx 31°$ for $E = 2.20$ eV.

where they are found to arise from interference between the time-direct (backward scattered) and time-delayed (forward scattered) N reaction mechanisms.

We can see other features in the LAM(θ_R, E) and LAM$_N$ (θ_R, E) contour plots in Figure 10 panels a and b, respectively, that could be indications of other, less well-defined reaction mechanism boundary lines (i.e., the subtle feature on the curve that starts at ($\theta_R \approx 68°$, $E = 1.52$ eV) and finishes at ($\theta_R \approx 0°$, $E = 1.70$ eV), as well as the numerous diagonal features that extend leftwards from the high E side of the (θ_R, E) plane in Figure 10b). The former feature occurs in a region where the DCS is very small and so is not likely to be of much physical interest, whereas the latter features correspond to the N-dominated oscillations with respect to θ_R observed in Figure 1 and mentioned previously in Section 4A.

The LAM$_F$(θ_R, E) contour plot in Figure 10c shows little information of discernible value, because $|f_F(\theta_R, E)|$ is generally much smaller than $|f(\theta_R, E)|$ and $|f_N(\theta_R, E)|$ (see Figures 1−6, 8, and 9). This also means the phase of $f_F(\theta_R, E)$ is contaminated by more numerical noise than are the phases of $f(\theta_R, E)$ and $f_N(\theta_R, E)$. The numerical noise is enhanced in LAM$_F$(θ_R, E) because of the differentiation operation in eqs 8 and 16.

Finally we consider the N,F LAM results at $E = 1.60$, 1.80, 2.00, and 2.20 eV in Figure 11 ($r = 0$) and Figure 12 ($r = 1$). Upon studying these figures, together with information gained from previous NF analyses of reactive scattering,[7,36,39−41] we note the following: (1) LAM(θ_R, E) is usually negative, corresponding to the scattering being dominated by repulsive

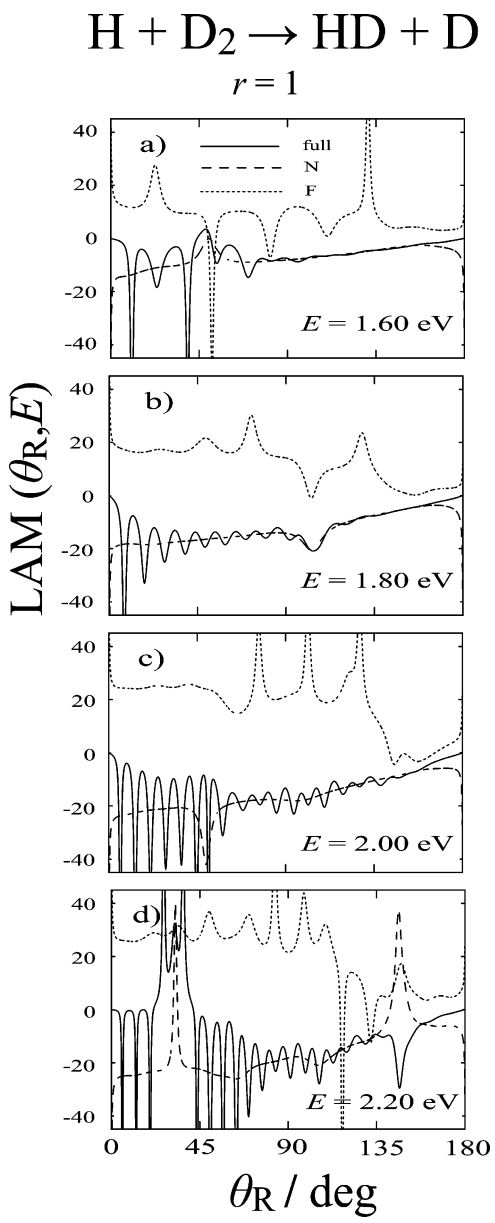

Figure 12. Plots of $\mathrm{LAM}(\theta_R, E)$ (solid curve), $\mathrm{LAM_N}(\theta_R, E)$ (dashed curve), and $\mathrm{LAM_F}(\theta_R, E)$ (dotted curve) vs θ_R, for resummation order, $r = 1$. (a) $E = 1.60$ eV, (b) $E = 1.80$ eV, (c) $E = 2.00$ eV, and (d) $E = 2.20$ eV. The trench−ridge structure occurs at (b) $\theta_R \approx 104°$ for $E = 1.80$ eV, (c) $\theta_R \approx 50°$ for $E = 2.00$ eV, and (d) $\theta_R \approx 31°$ for $E = 2.20$ eV.

N interactions. (2) $\mathrm{LAM}(\theta_R, E)$ possesses oscillations, which damp out as θ_R increases. In contrast, the $\mathrm{LAM_{N,F}}(\theta_R, E)$ and $\mathrm{LAM_{N,F}}(\beta_1;\theta_R, E)$ curves are more slowly varying, which means the oscillations in $\mathrm{LAM}(\theta_R, E)$ are an NF interference effect. Resummation ($r = 1$, Figure 12) helps to clean the $r = 0$ $\mathrm{LAM_N}(\theta_R, E)$ and $\mathrm{LAM_F}(\theta_R, E)$ curves in Figure 11 of unphysical oscillations. (3) At small angles, the F LAM curves are approximately constant at the three higher energies. For example, at $E = 2.00$ eV, $\mathrm{LAM_F}(\theta_R, E) \approx 24$ for $4° \lesssim \theta_R \lesssim 40°$, which means that partial waves with $J \approx 24$ are dynamically important for scattering into forward angles at this energy. At larger angles, the F LAM curves possess pronounced oscillations. However, these occur where $|f_F(\theta_R, E)|$ and $|f_F(\beta_1; \theta_R, E)|$ are much smaller that the moduli of the full and N scattering amplitudes (see Figures 2−5). Hence, these large angle F oscillations are not physically meaningful. (4) The $\mathrm{LAM_N}(\theta_R, E)$ and $\mathrm{LAM_N}(\beta_1; \theta_R, E)$ decrease approximately monotonically, with the exception of the trench−ridge structure, as θ_R increases. This is expected for a reaction in which the N scattering is dominated by repulsive interactions. In particular, the N LAM for the classical scattering of two hard spheres, $\mathrm{LAM_N}(\theta_R, E) = -kd \cos(\theta_R/2)$, where d is the sum of their radii, provides a first approximation to the N LAM curves in Figures 11 and 12. (5) An example of possibly unphysical N behavior is the appearance in Figure 12d of a large spike in the $r = 1$ $\mathrm{LAM_N}(\beta_1; \theta_R, E)$ at ($\theta_R \approx 145°$, $E = 2.20$ eV). Further resummation (not shown) makes this feature disappear again, and so it is not physical. (6) We do see an example of true F dominance (which is well-behaved and does not disappear upon resummation, i.e., upon going from $r = 0$ to $r = 1$) in $\mathrm{LAM}(\theta_R, E)$: the two positive peaks on either side of the ridge structure at ($\theta_R \approx 30°$, $E = 2.20$ eV) in Figures 11d ($r = 0$) and 12d ($r = 1$). This may be an indication that there are more than two reaction mechanisms interfering in this angular region, because this feature is different from the N-dominated trench−ridge structure. Note that F scattering also dominates in the corresponding NF DCS plots for ($\theta_R \approx 30°$, $E = 2.20$ eV), see Figures 3d ($r = 0$) and 5d ($r = 1$). (7) Upon comparing the NF oscillations in the LAM curves in Figures 11 and 12 with the corresponding oscillations in the DCS plots in Figures 2−5, we find they are similar, although more pronounced in the LAM case. This provides a consistency check on our NF interpretation of structure in the plots of $\sigma(\theta_R, E)$. (8) The relation between $\mathrm{LAM_N}(\theta_R, E)$, $\mathrm{LAM_F}(\theta_R, E)$, and $\mathrm{LAM}(\theta_R, E)$ is given by the fundamental NF identity for LAMs, which can be written in the form shown in eq 26

$$\mathrm{LAM}(\theta_R, E) = \frac{[\sigma_N(\theta_R, E)\,\mathrm{LAM_N}(\theta_R, E) + \sigma_F(\theta_R, E)\,\mathrm{LAM_F}(\theta_R, E) + C(\theta_R, E)]}{|f_N(\theta_R, E) + f_F(\theta_R, E)|^2} \qquad (26)$$

and is also true for the resummed N and F LAMs. In eq 26, the term $C(\theta_R, E)$ is usually small in magnitude; it is defined explicitly in ref 40. A detailed examination of the properties of the identity (eq 26) for the $E = 2.00$ eV case has been reported earlier, making use of the concept of a cross section × LAM (CLAM) plot.[40]

6. Conclusions

We have presented the results of time-independent NF DCS and NF LAM analyses for the H + D_2 ($v_i = 0$, $j_i = 0$, $m_i = 0$) → HD ($v_f = 3$, $j_f = 0$, $m_f = 0$) + D reaction. We showed that the energy-domain analog of the time-direct (backward-scattered) reaction mechanism is N dominated, whereas the time-delayed (forward-scattered) analog is a result of NF interference. These findings are in accordance with the time-domain analyses of ref 7.

We showed that resumming the PWS for the scattering amplitude generally improves the physical meaning of the N,F DCSs and the N,F LAMs. We presented two examples where the physical significance of the NF analysis did not improve upon resummation, namely, for ($E = 2.00$ eV and $r = 2$) and ($E = 2.18$ eV and $r = 1$), where unphysically large peaks appear over a small angular range in the $\sigma_N(\boldsymbol{\beta}; \theta_R, E)$ and $\sigma_F(\boldsymbol{\beta}; \theta_R, E)$ versus θ_R graphs. It was demonstrated that this behavior is caused by the modulus of the presummation factors taking large values and can be reduced by moving the Im β_i away from zero when $|\mathrm{Re}\ \beta_i| > 1$.

Our NF LAM results contain information complementary to that in NF DCS plots. In particular, structure in the NF LAM-(θ_R, E) data, such as the trench−ridge feature, is useful for

highlighting regions in (θ_R, E) space where different reaction mechanisms interfere.

Acknowledgment. Support of this research by the U.K. Engineering and Physical Sciences Research Council is gratefully acknowledged. We also thank the Royal Society, London for the award of a University Research Fellowship to S. C. A.

References and Notes

(1) Hu, W.; Schatz, G. C. *J. Chem. Phys*. **2006**, *125*, 132301.
(2) *Semiclassical and Other Methods for Understanding Molecular Collisions and Chemical Reactions*; Sen, S., Sokolovski, D., Connor, J. N. L., Eds.; Collaborative Computational Project on Molecular Quantum Dynamics (CCP6), Daresbury Laboratory: Warrington, United Kingdom, 2005.
(3) *Theory of Chemical Reaction Dynamics*, Proceedings of the NATO Advanced Research Workshop on Theory of the Dynamics of Elementary Chemical Reactions, Balatonföldár, Hungary, 8−12 June, 2003; Laganà, A., Lendvay, G., Eds. Kluwer: Dordrecht, The Netherlands, 2004.
(4) *Modern Trends in Chemical Reaction Dynamics, Experiment and Theory*; Parts I and II; Yang, X.; Liu, K., Eds.; World Scientific: Singapore, 2004.
(5) Althorpe, S. C.; Clary, D. C. *Annu. Rev. Phys. Chem*. **2003**, *54*, 493.
(6) Nyman, G.; Yu, H.-G. *Rep. Prog. Phys.* **2000**, *63*, 1001.
(7) Monks, P. D. D.; Connor, J. N. L.; Althorpe, S. C. *J. Phys. Chem. A* **2006**, *110*, 741.
(8) Althorpe, S. C.; Fernández-Alonso, F.; Bean, B. D.; Ayers, J. D.; Pomerantz, A. E.; Zare, R. N.; Wrede, E. *Nature* **2002**, *416*, 67.
(9) Althorpe, S. C. *J. Chem. Phys*. **2002**, *117*, 4623.
(10) Althorpe, S. C. *Chem. Phys. Lett.* **2003**, *370*, 443.
(11) Althorpe, S. C. *J. Phys. Chem. A* **2003**, *107*, 7152.
(12) Juanes-Marcos, J. C.; Althorpe, S. C. *Chem. Phys. Lett.* **2003**, *381*, 743.
(13) Althorpe, S. C. *Phys. Rev. A* **2004**, *69*, 042702.
(14) Althorpe, S. C. *J. Chem. Phys*. **2004**, *121*, 1175.
(15) Althorpe, S. C. *Int. Rev. Phys. Chem.* **2005**, *23*, 219.
(16) Althorpe, S. C. In *Semiclassical and Other Methods for Understanding Molecular Collisions and Chemical Reactions*; Sen, S., Sokolovski, D., Connor, J. N. L., Eds.; Collaborative Computational Project on Molecular Quantum Dynamics (CCP6), Daresbury Laboratory: Warrington, United Kingdom, 2005; pp 58−61.
(17) Connor, J. N. L.; McCabe, P.; Sokolovski, D.; Schatz, G. C. *Chem. Phys. Lett.* **1993**, *206*, 119.
(18) Sokolovski, D.; Connor, J. N. L.; Schatz, G. C. *Chem. Phys. Lett.* **1995**, *238*, 127.
(19) Sokolovski, D.; Connor, J. N. L.; Schatz, G. C. *J. Chem. Phys.* **1995**, *103*, 5979.
(20) McCabe, P.; Connor, J. N. L. *J. Chem. Phys.* **1996**, *104*, 2297.
(21) Sokolovski, D.; Connor, J. N. L.; Schatz. G. C. *Chem. Phys.* **1996**, *207*, 461.
(22) Wimp, J.; McCabe, P.; Connor, J. N. L. *J. Comput. Appl. Math.* **1997**, *82*, 447.
(23) McCabe, P.; Connor, J. N. L.; Sokolovski, D. *J. Chem. Phys.* **1998**, *108*, 5695.
(24) Sokolovski, D.; Connor, J. N. L. *Chem. Phys. Lett.* **1999**, *305*, 238.
(25) Hollifield, J. J.; Connor, J. N. L. *Phys. Rev. A* **1999**, *59*, 1694.
(26) Hollifield, J. J.; Connor, J. N. L. *Mol. Phys.* **1999**, *97*, 293.
(27) Dobbyn, A. J.; McCabe, P.; Connor, J. N. L.; Castillo, J. F. *Phys. Chem. Chem. Phys.* **1999**, *1*, 1115.
(28) Vrinceanu, D.; Msezane, A. Z.; Bessis, D.; Connor, J. N. L.; Sokolovski, D. *Chem. Phys. Lett.* **2000**, *324*, 311.
(29) McCabe, P.; Connor, J. N. L; Sokolovski, D. *J. Chem. Phys.* **2001**, *114*, 5194.
(30) Whiteley, T. W. J.; Noli, C.; Connor, J. N. L. *J. Phys. Chem. A* **2001**, *105*, 2792.
(31) Noli, C.; Connor, J. N. L.; Rougeau, N.; Kubach, C. *Phys. Chem. Chem. Phys.* **2001**, *3*, 3946.
(32) Noli, C.; Connor, J. N. L. *Russ. J. Phys. Chem.* **2002**, *76*, Supplement 1, S77.
(33) Anni, R.; Connor, J. N. L.; Noli, C. *Phys. Rev. C* **2002**, *66*, 044610.
(34) Anni, R.; Connor, J. N. L.; Noli, C. *Khim. Fiz*. **2004**, *23*, No. 2, 6.
(35) Connor, J. N. L. *Phys. Chem. Chem. Phys.* **2004**, *6*, 377.
(36) Connor, J. N. L.; Anni, R. *Phys. Chem. Chem. Phys.* **2004**, *6*, 3364.
(37) Connor. J. N. L. *Mol. Phys*. **2005**, *103*, 1715.
(38) Xiahou, C.; Connor, J. N. L. In *Semiclassical and Other Methods for Understanding Molecular Collisions and Chemical Reactions*; Sen, S., Sokolovski, D., Connor, J. N. L., Eds.; Collaborative Computational Project on Molecular Quantum Dynamics (CCP6), Daresbury Laboratory: Warrington, United Kingdom, 2005; pp 44−49.
(39) Xiahou, C.; Connor, J. N. L. *Mol. Phys*. **2006**, *104*, 159.
(40) Monks, P. D. D.; Xiahou, C.; Connor, J. N. L. *J. Chem. Phys.* **2006**, *125*, 133504.
(41) Monks, P. D. D.; Connor, J. N. L.; Althorpe, S. C. In *Semiclassical and Other Methods for Understanding Molecular Collisions and Chemical Reactions;* Sen, S., Sokolovski, D., Connor, J. N. L., Eds.; Collaborative Computational Project on Molecular Quantum Dynamics (CCP6), Daresbury Laboratory: Warrington, United Kingdom, 2005; pp 112−118.
(42) Sokolovski, D.; Castillo, J. F.; Tully, C. *Chem. Phys. Lett.* **1999**, *313*, 225.
(43) Sokolovski, D.; Castillo, J. F. *Phys. Chem. Chem. Phys.* **2000**, *2*, 507.
(44) Sokolovski, D. *Phys. Rev. A* **2000**, *62*, 024702.
(45) Aoiz, F. J.; Bañares, L.; Castillo, J. F.; Sokolovski, D. *J. Chem. Phys.* **2002**, *117*, 2546.
(46) Sokolovski, D. *Russ. J. Phys. Chem*. **2002**, *76*, Supplement 1, S21.
(47) Sokolovski, D. *Chem. Phys. Lett.* **2003**, *370*, 805.
(48) Sokolovski, D.; Msezane, A. Z. *Phys. Rev. A* **2004**, *70*, 032710.
(49) Sokolovski, D.; Sen, S. K.; Aquilanti, V.; Cavalli, S.; De Fazio, D. *J. Chem. Phys*. **2007**, *126*, 084305.
(50) Juanes-Marcos, J. C.; Althorpe, S. C.; Wrede, E. *Science* **2005**, *309*, 1227. For a commentary, see Clary, D. C. *Science* **2005**, *309*, 1195.
(51) Panda, A. N.; Althorpe, S. C. *Chem. Phys. Lett.* **2006**, *419*, 245.
(52) Juanes-Marcos, J. C.; Althorpe, S. C.; Wrede, E. *J. Chem. Phys.* **2007**, *126*, 044317.
(53) Panda, A. N.; Althorpe, S. C. *Chem. Phys. Lett.* **2007**, *439*, 50.
(54) Althorpe, S. C.; Juanes-Marcos, J. C.; Wrede, E. *Adv. Chem. Phys.* In press.
(55) Guillon, G.; Stoecklin, T. *Eur. Phys. J. D* **2006**, *39*, 359.
(56) Schatz, G. C. In *Advances in Classical Trajectory Methods*; Hase, W. L. Ed.; JAI Press: Stamford, Connecticut, 1998; Vol. 3, pp 205−229.
(57) Boothroyd, A. I.; Keogh, W. J.; Martin, P. G.; Peterson, M. R. *J. Chem. Phys.* **1996**, *104*, 7139.
(58) Aoiz, F. J.; Bañares, L.; Herrero, V. J. *Int. Rev. Phys. Chem*. **2005**, *24*, 119.
(59) Bañares, L.; Aoiz, F. J.; Herrero, V. J. *Phys. Scr*. **2006**, *73*, C6.
(60) Fuller, R. C. *Phys. Rev. C* **1975**, *12*, 1561.
(61) Althorpe, S. C. *J. Chem. Phys.* **2001**, *114*, 1601.
(62) Pomerantz, A. E.; Ausfelder, F.; Zare, R. N.; Althorpe, S. C.; Aoiz, F. J.; Bañares, L.; Castillo, J. F. *J. Chem. Phys.* **2004**, *120*, 3244.
(63) Ausfelder, F.; Pomerantz, A. E.; Zare, R. N.; Althorpe, S. C.; Aoiz, F. J.; Bañares, L.; Castillo, J. F. *J. Chem. Phys.* **2004**, *120*, 3255.
(64) Pomerantz, A. E.; Ausfelder, F.; Zare, R. N.; Juanes-Marcos, J. C.; Althorpe, S. C.; Sáez Rábanos, V.; Aoiz, F. J.; Bañares, L.; Castillo, J. F. *J. Chem. Phys.* **2004**, *121*, 6587.
(65) Juanes-Marcos, J. C.; Althorpe, S. C. *J. Chem. Phys.* **2005**, *122*, 204324.
(66) Koszinowski, K.; Goldberg, N. T.; Pomerantz, A. E.; Zare, R. N.; Juanes-Marcos, J. C.; Althorpe, S. C. *J. Chem. Phys.* **2005**, *123*, 054306.
(67) Dai, D.; Wang, C. C.; Harich, S. A.; Wang, X.; Yang, X.; Chao, S. D.; Skodje, R. T. *Science* **2003**, *300*, 1730.